Microstructural variations of poly(vinylidene fluoride co-hexafluoropropylene) and their influence on the thermal, dielectric and piezoelectric properties

R.E. Sousa [a], J. Nunes-Pereira [a], J.C.C. Ferreira [a], C.M. Costa [a], A.V. Machado [b], M.M. Silva [c], S. Lanceros-Mendez [a,*]

[a] Departamento/Centro de Física, Universidade do Minho Campus de Gualtar, 4710-057 Braga, Portugal

[b] IPC - Institute for Polymers and Composites, Universidade do Minho, Campus de Azurém, 4800-058 Guimarães, Portugal

[c] Departamento/Centro de Química, Universidade do Minho Campus de Gualtar, 4710-057 Braga, Portugal

Keywords:

PVDF-HFP
Membranes
Thermally induced phase separation (TIPS)
Phase diagram

Abstract

Polymer films and membranes of poly(vinylidene fluoride co-hexafluoropropylene), PVDFHFP, have been prepared by thermally induced phase separation (TIPS), allowing the tuning of microstructure and morphology. The obtained microstructure is explained by the Flory-Huggins theory, depending on polymer concentration and solvent evaporation temperature. The formation of a porous membrane is attributed to a spinodal decomposition of the liquid-liquid phase separation. The effect of the processing conditions on the morphology, degree of porosity, degree of crystallinity and crystalline polymorph, thermal, dielectric and piezoelectric properties of the PVDF-HFP polymer were evaluated. The crystalline phase and degree of crystallinity depend on the processing conditions and further

influence the dielectric and piezoelectric response. The piezoelectric coefficient is correlated with the β-phase content and decreases with decreasing polymer concentration in the initial solution at a given evaporation temperature.

Introduction

Significant advances are being made in scientific and commercial areas for the development of membrane technologies [1]. Polymeric membranes are being used for a variety of areas, including microfiltration (MF) [2], ultrafiltration (UF) [1,2], reverse osmosis (RO) [1,2], nanofiltration (NF) [3], hyperfiltration [3] and gas separation [2]. The applications of membrane technologies cover almost every industrial sector including fuel cell technologies [4], lithium-ion batteries [1,5] and membrane distillation (MD) [6].

Each application imposes specific requirements for the membrane material and structure in terms, of porosity and pore size [2], anti-fouling properties, mechanical strength and chemical resistance [1], the final properties of the polymer membrane depending strongly on processing parameters [7,8].

The most commonly used technique to produce membranes is phase separation of polymer solutions by phase inversion [2]. This separation can be accomplished by different methods including thermally induced phase separation (TIPS) [9], controlled evaporation of solvent [10], precipitation from the vapour phase [11], immersion precipitation (IP) [12] and air-casting [13]. Currently, most of the commercial membranes for microfiltration and ultrafiltration [14] are produced by phase inversion methods [14], mainly due to its simplicity and flexible production scale.

TIPS has become one of the main methods used for polymer membrane preparation [15], as it shows some advantages in comparison to traditional phase separation processes: it can be applied to a wide range of polymers [9]; can be used to generate dense and porous films, the latter with isotropic, anisotropic or asymmetric microstructures with an overall porosity as high as 90%; and it is more flexible than wet or dry-casting, since it depends primarily on heat transfer rather than multi-component mass transfer [9].

Poly(vinylidene fluoride) (PVDF) has received much attention as a membrane material due to its outstanding properties such as high mechanical strength, thermal stability, chemical resistance and high hydrophobicity, when compared to other polymer materials, such as polysulfone (PSU), polyethersulfone (PES) and polyimide (PI) [16].

PVDF membranes have been extensively applied in ultrafiltration and microfiltration [17], and are currently being explored as candidates in membrane contactor [18] and membrane distillation applications [19]. PVDF dissolves in common organic solvents, from which porous PVDF membranes can be produced by phase inversion [20].

Besides PVDF, there are other fluoropolymers that can be used as membrane materials, such as poly(vinylidenefluoride-co-hexafluoropropylene) (PVDFHFP) and poly(vinylidenefluoride-trifluoroethylene) (PVDFTrFE) [20]. PVDF-HFP has drawn much attention [1,21] and seems to be more promising than PVDF for membrane applications. The addition of the amorphous phase related to the hexafluropropylene (HFP) group to the main VDF blocks increases the fluorine content, leading to a more hydrophobic material [1], soluble in more solvents and with lower degree of crystallinity [22].

Microporous membranes of PVDF-HFP have been prepared by phase inversion from acetone/water/PVDF-HFP solutions with degrees of porosity between 70 and 90% [23].

The effect of PVDF-HFP concentration for the development of hollow fiber membranes has been studied in the system N,N-dimethylacetamide (DMA_C)/ poly (ethylene glycol)/(PEG)/PVDF-HFP, and it was verified that internal and external pore sizes decreased with increasing copolymer content [24].

PVDF-HFP membranes were also produced from PVDF and propylene carbonate (PC) or dimethyl sulfoxide (DMSO) solutions, the gelation occurring at relatively low concentrations and the miscibility area of the ternary diagram being larger for DMSO [25].

Taking into account the reported literature for production of membranes based on PVDF-HFP, a systematic approach to the modification of PVDF-HFP microstructure is still needed. Thus, the present work is devoted to the preparation of membranes from the PVDF-HFP/N,N dimethylformamide (DMF) solution by TIPS. Membranes with different microstructures have been obtained and characterized.

Experimental

Materials

Poly(vinylidene fluoride-co-hexafluropropylene) P(VDFHFP) (Solef 21216; M_w = 600,000 g/mol; 12wt.%HFP) was supplied by Solvay. N,N-dimethylformamide (DMF, 99.5%) was supplied by Merck.

Membrane preparation

The polymer was dissolved in DMF at room temperature under constant magnetic stirring until a homogeneous solution was obtained. The PVDF-HFP polymer concentration in solution ranged from 5wt.% to 20wt.%. After total polymer dissolution, the solution was placed on a clean glass substrate and spread by blade coating with a thickness of 100μ m, followed by isothermal evaporation in an air oven at temperatures from room to 100°C.

Sample characterization

The morphology of the PVDF-HFP membranes was obtained by scanning electron microscopy (SEM) (Cambridge, Leica) with an accelerating voltage of 15 kV . The samples were previously coated with a thin gold layer using a sputter coating (Polaron, model SC502 sputter coater).

The porosity of the membranes was determined from the membrane (ρ_m) and pristine polymer densities ($\rho_{pol} = 1.77$ g/cm^3) [26] using a pycnometer:

$$\rho_m = \frac{\rho_w m_3}{m_1 + m_3 - m_2} \quad (1)$$

where ρ_w is the water density, m_1 is the mass of pycnometer with water, m_2 is the mass of pycnometer with water and the membrane and m_3 is the mass of the dry membrane.

The degree of porosity was then calculated from [26]:

$$\phi = 1 - \frac{\rho_{\mathrm{m}}}{\rho_{\mathrm{pol}}} \tag{2}$$

Contact angle measurements (sessile drop in dynamic mode) were performed at room temperature in a Data Physics OCA20 device using ultrapure water (3 mL droplets) as the test liquid. At least 3 measurements on each sample were performed in different sample locations and the average contact angle was calculated.

The polymer crystalline form was identified by Fourier Transformed Infrared spectroscopy (FTIR) at room temperature with a Jasco FT/IR-4100. FTIR spectra were collected in attenuated total reflectance mode (ATR) from 4000 to 600 cm^{-1} after 32 scans with a resolution of 4 cm^{-1}.

Melting temperature and degree of crystallinity were determined by differential scanning calorimetry (DSC) with a Mettler Toledo 821e apparatus. The samples were cut from the central region of the membranes, placed in 50μ L crucibles and heated from 50 to 200°C at a rate of 10°C/ min, under an argon atmosphere. The degree of crystallinity (χ_c) was calculated from the enthalpy of the melting peak ($\Delta \mathrm{H_f}$) based on the enthalpy of a 100% crystalline sample, through the following equation:

$$\chi_C = \frac{\Delta H_f}{x\Delta H_\alpha + y\Delta H_\beta} \tag{3}$$

where x is the weight fraction of the α phase, y is the weight fraction of the β phase determined from the FTIR measurements (Fig. 2a), ΔH_α is the melting enthalpy of pure crystalline α-PVDF and ΔH_β is the melting enthalpy of pure crystalline β-PVDF which are reported to be 93.04 J/g and 103.4 J/g, respectively [27,28].

Dielectric measurements were performed using a Quadtech 1920 LCR precision meter. The real part of the dielectric function (ε') and the dielectric losses (tan δ) were obtained at room temperature in the frequency range of 20 Hz to 1 MHz with an applied voltage of 0.5 V . Circular aluminum electrodes of 5 mm diameter were vacuum evaporated onto both sides of each sample. The error associated with the dielectric measurements is ~ 2%, mainly due to the geometrical factors.

The piezoelectric $\mathrm{d_{33}}$ coefficients were then measured using a $\mathrm{d_{33}}$ meter APC YE2730A.

The PVDF-HFP was first poled by corona discharge at a controlled temperature inside a home-made corona chamber with the following parameters: applied voltage of 10 kV at a constant current of 20μ A; constant distance of 2 cm between the sample and the tip; poling time 30 min . The poling conditions were further optimized by varying poling temperature from 80 to 120°C and then cooled to room temperature under the applied electric field [29].

Results

The membrane thickness varied between $9 - 76\mu$ m depending on polymer concentration (Fig. 1) and was independent of the evaporation temperature.

SEM images showing the microstructural evolution of the PVDF-HFP samples prepared by solvent evaporation at room temperature and varying initial polymer concentration from 5 to 20wt. % are presented in Fig. 2 a)-d).

The membranes show a porous morphology evolving from large pore sizes of $\sim 7.5\mu$ m (Fig. 2a) to lower pore sizes of $\sim 2\mu$ m (Fig. 2d), the pore size decreasing with increasing initial polymer concentration in the PVDF-HFP/DMF solution.

In particular, Fig. 2a) shows a three dimensional particulate morphology with macro voids or finger-like pores, suggesting a precipitation situation dominated by liquid-

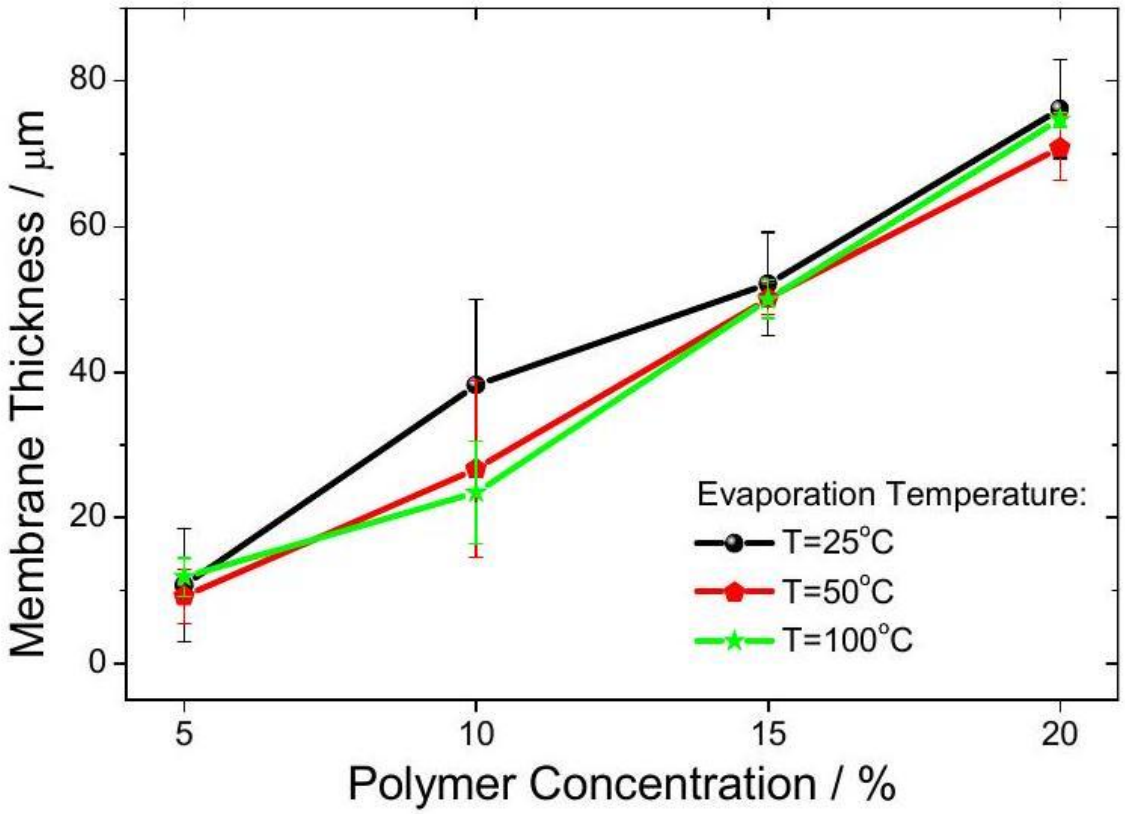

Fig. 1. Membrane thickness as a function of polymer concentration for the different evaporation temperatures.

liquid demixing in the phase diagram [30]. The inset of Fig. 2a, shows that the particulate morphology is the spherulitic structure characteristic of PVDF [31].

The degree of porosity of the PVDF-HFP membranes is plotted in Fig. 3 as a function of initial polymer concentration.

Regardless of initial polymer concentration, the membranes show high degrees of porosity between 56% and 78% for 15 and 10wt% of PVDF-HFP, respectively, which is in line with the degree of porosity obtained in similar systems (PVDF-HFP/DMF/clay) [32]. The high

degree of porosity is due to the low evaporation temperature, the polymer chains have reduced mobility and prevent the polymer from occupying the free space left by the evaporated solvent [33]. These effects will be later discussed relative to the phase diagram of PVDF-HFP/DMF system.

The effect of the solvent evaporation temperature on membrane morphology is shown in Figs. 2 e-f). The presence of pores is not observed for membranes with 20wt.% of initial polymer concentration with solvent evaporation temperatures of 50°C and 100°C, Fig. 2e) and 2f), respectively. The morphology of these membranes is characterized by a dense and compact microstructure. Increasing solvent evaporation temperature above of 40°C increased polymer chain mobility, making them able to occupy the free space left by the solvent during evaporation, which results in a compact microstructure. Further, increasing temperature leads to increased solvent evaporation rate and favors polymer diffusion and spherulite growth [34]. The spherulite size increases with increasing evaporation temperature for a given polymer concentration (Figs. 2a, 2e) and f). At solvent evaporation temperatures above 40°C, the morphology of the membranes is independent of the polymer concentration.

Fig. 3 presents the variation of porosity as a function of polymer concentration in the PVDF-HFP/DMF system at room temperature, which varies between 55 and 75%. One important parameter for the development of membrane applications is the hydrophobicity of the membranes, which can be assessed through measurement of the contact angle. The contact angle as a function of initial polymer concentration and for the different evaporation temperatures is illustrated in the Fig. 4. For membranes up to 10wt.% initial polymer concentration with solvent evaporation at room temperature, a water contact angle above 125° is measured, which is related to the large pore size and irregular surface [35]. Increasing initial polymer concentration leads to a strong decrease of the contact angle to ~ 85° due to the smoother and more compact morphology (Fig. 1) [36].

Increasing solvent evaporation temperature leads to a strong decrease of the water contact angle to values around 85°, which increases up to ~ 95° for increasing initial polymer concentration, associated with increased roughness in this compact morphology, related to the larger spherulite sizes (Fig. 2) as discussed in [37].

The crystalline phase of the polymer is relevant for the different applications of this electroactive polymer [20] and can be determined by FTIR. Table 1 shows the most relevant vibration modes of PVDF-HFP and Fig. 5 shows the FTIRATR spectra of the membranes.

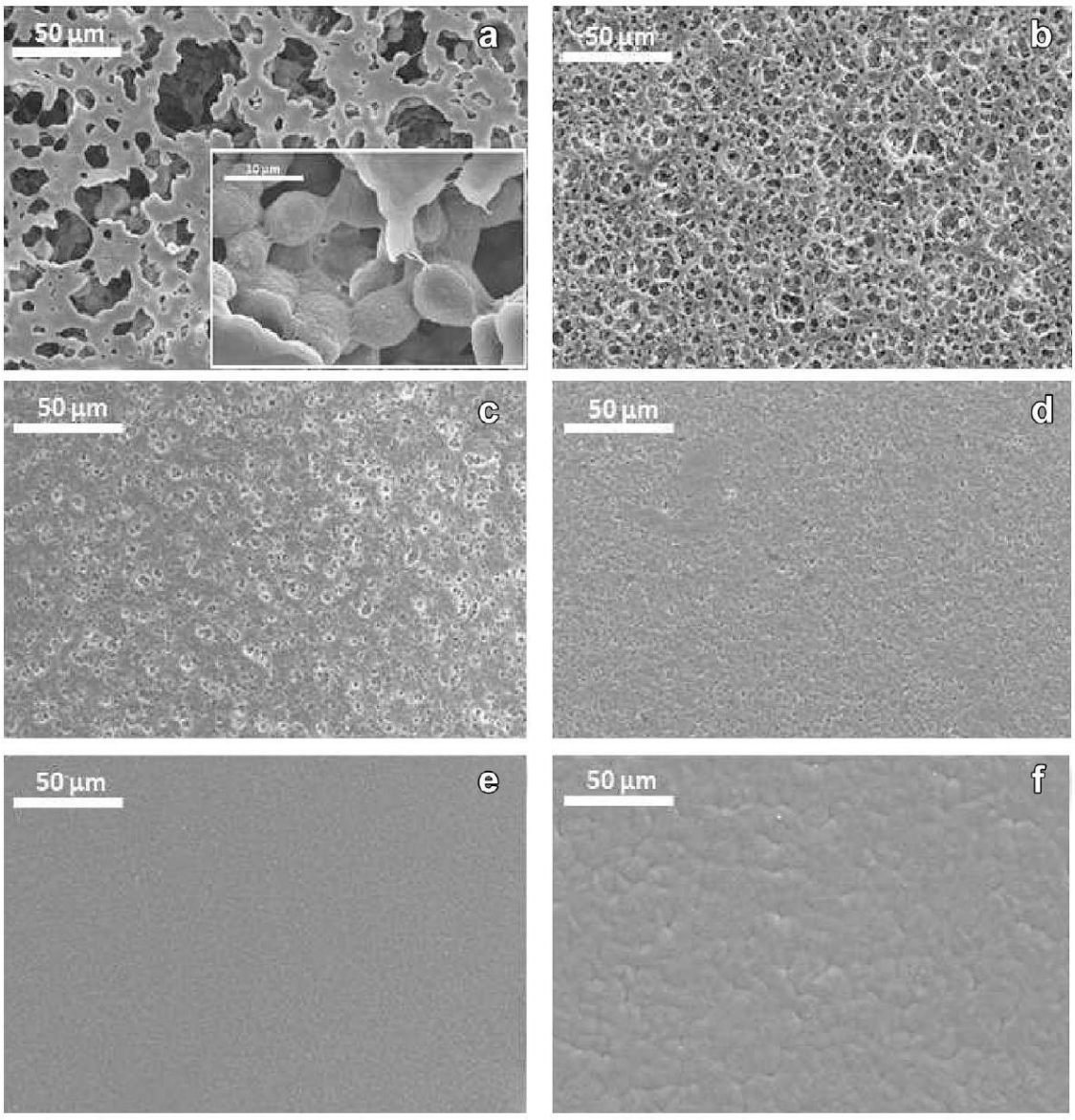

Fig. 2. Surface images of the PVDF-HFP membranes prepared from the PVDF-HFP/DMF solution: solvent evaporation at room temperature with 5 wt.% PVDF-HFP (a), 10wt. % PVDF-HFP (b), 15wt. % PVDF-HFP (c) and 20wt. % of PVDF-HFP (d). Microstructures of the sample with 20wt. % PVDF-HFP with solvent evaporation at 50°C (e) and 100°C (f).

In particular, Fig. 5a) shows the FTIR-ATR spectra for the sample prepared from 20wt. % PVDF-HFP in the PVDF-HFP/ DMF system for the different solvent evaporation temperatures, and Fig. 5 b) shows the spectra for the samples

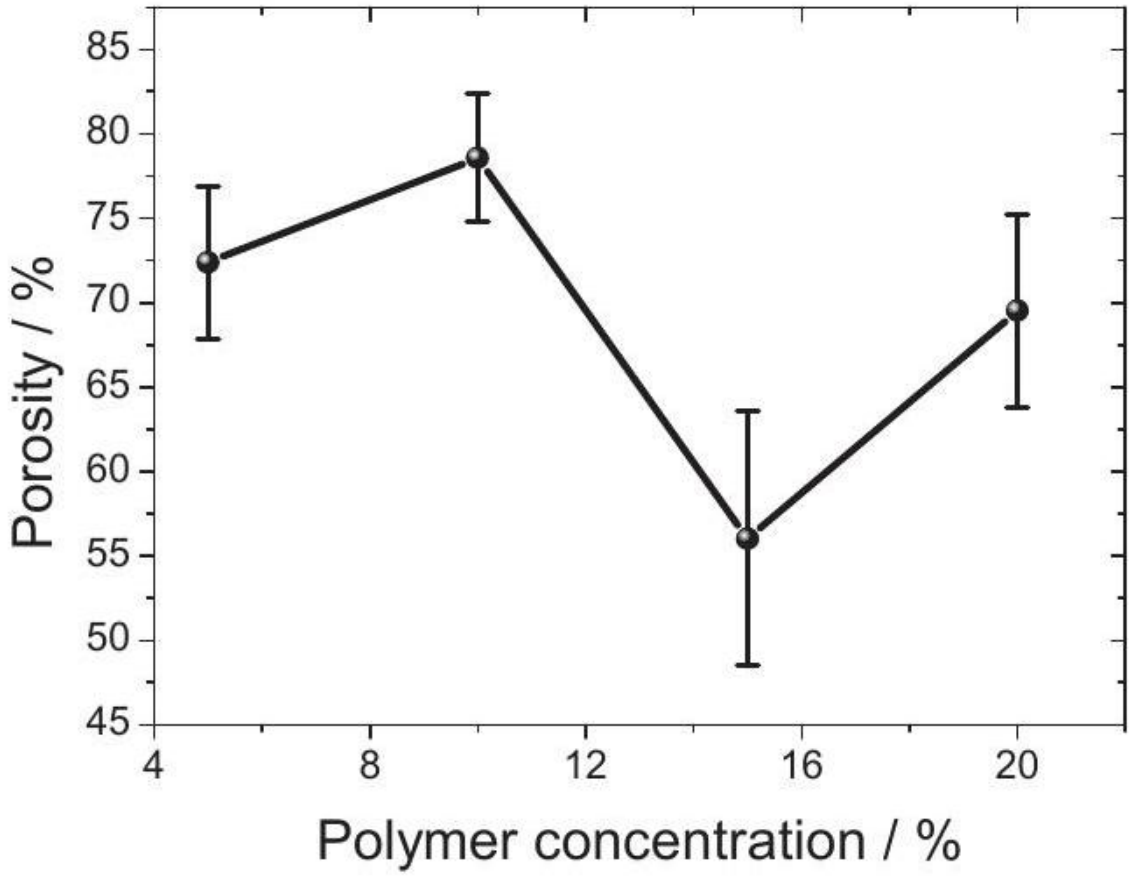

Fig. 3. Degree of porosity as a function of PVDF-HFP initial concentration in the PVDF-HFP/DMF system prepared by solvent evaporation at room temperature. obtained at 100 °C solvent evaporation temperature for different initial polymer contents.

Most relevant bands (Table 1) are clearly identified in all the spectra, indicating no significant variations in the polymer structure. The arrows in Fig. 5 represent the

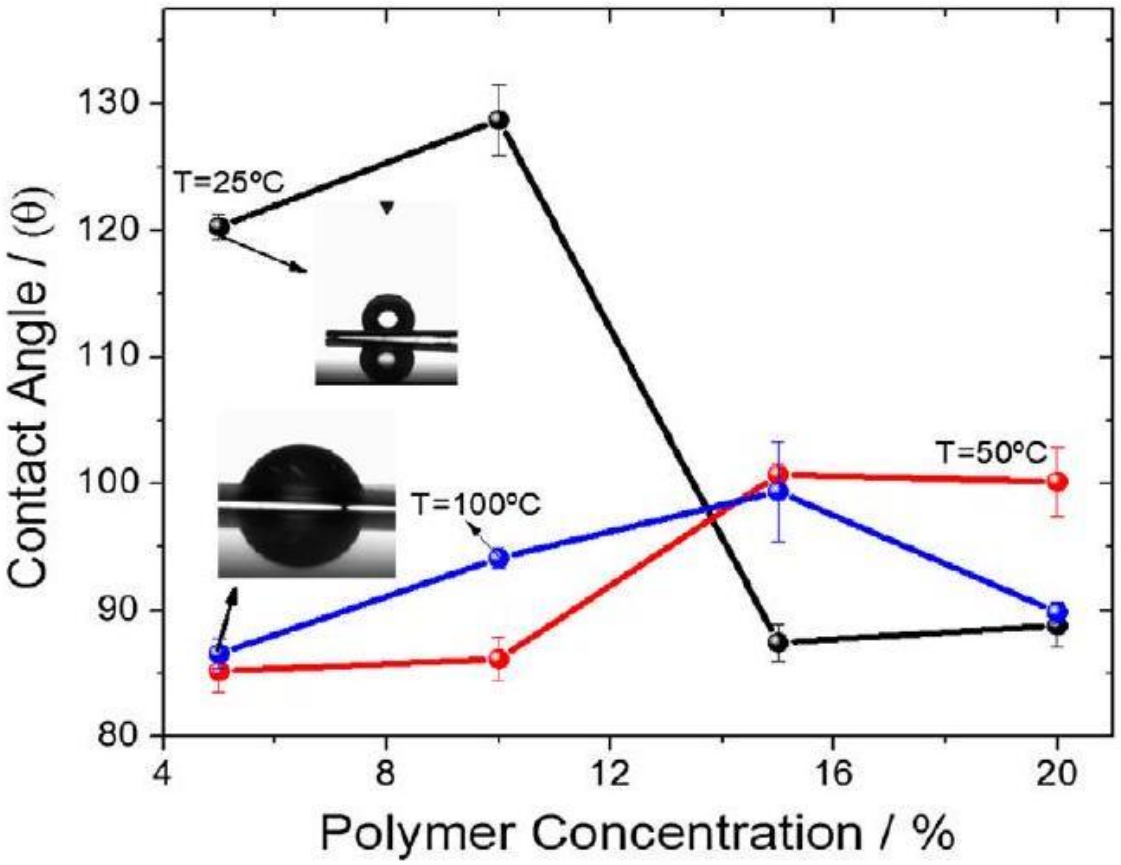

Fig. 4. Contact angle as a function of PVDF-HFP concentration for the different evaporation temperatures.

Table 1
Vibration modes characteristics of the PVDF-HFP polymer where $\boldsymbol{v_s}$ is symmetric stretching, $\boldsymbol{v_a}$ is antisymmetric stretching, $\boldsymbol{\delta}$ is scissoring, **w** is wagging, **t** is twisting, **r** is rocking, CCC δ is skeletal bending of $C(F)-C(H)-C(F)$ and $CCC\delta'$ is skeletal bending of $C(H)-C(F)-C(H)$.

Wavenumber (cm^{-1})	Vibration modes	Ref
611	- C – F-wagging modes	[38]
613	$CF_2(\delta)$ and CCC δ'	[39]
615	α-phase	[27]
760	α-phase	[40]
762	$CF_2(\delta)$ and CCC δ	[39]
765	α-phase	[41]
766	α-phase	[42]

794	CF_3 stretching	[40]
795	α-phase	[40]
796	CF_3 stretching	[38]
798	CH_2 (r)	[39]
834	CH_2 (r)	[39]
836	Amorphous region	[40]
838	β phase	[43]
839	Amorphous phase	[42]
841	γ-phase	[42]
853	α-phase	[40]
871	amorphous phase	[43]
877	CC (v_s) and CCC δ	[39]
879	Amorphous phase	[42]
974-976	α-phase	[40,42,43]
977	α-phase (due to TGTG-(T: trans and G: gauche) conformation)	[38]
978	CH_2 (t)	[39]
1062	C-C skeletal vibration	[40]
1063	symmetrical stretching mode of CF_2	[43]
1069	CF_2 (vs) and CH_2 (w)	[39]
1148	symmetrical stretching mode of CF_2	[43]
1151	$CC(v_a)$ and $CF_2(v_s)$	[39]
1173	Symmetrical stretching mode of CF_2	[44]
1179	Symmetrical stretching mode of CF_2	[43]
1185	$CF_2(v_s) + CH_2(t)$	[39]
1197	asymmetric stretching vibrations of the $-CF_2$ group	[42]
1200	$-CF_2$ groups	[44]
1202	Asymmetrical stretching of $-CF_2-$	[40]

1203	asymmetrical stretching vibrations of the CF_2 group	[43]
1212	α-phase	[40]
1214	$CF_2(v_a) + CH_2(w)$	[39]
1276	symmetric stretching vibrations of the $-CF_2$ group	[42]
1295	$CF_2(v_a)$ and $CF_2(r)$	[39]
1382	symmetrical stretching mode of CH_2 wagging	[43]
1384	α-phase	[40]
1386	$CH_2(\delta) + CH_2(w)$	[39]
1390	CH_2 groups	[44]
1400	$-C-F-$ stretching	[40]
1401	$CH_2(\delta)$, $CH_2(w)$, and CC (v_a)	[39]
1402	- CF groups	[44]
2924	$CH_2(v_s)$	[39]
2982	$CH_2(v_s)$	[39]
3025	$CH_2(v_a)$	[39]

vibrational bands at 760,974,1148,1295 and 1384 cm^{-1} which show higher variation depending on sample preparation procedure. The peaks at 760,974 and 1384 cm^{-1} correspond to α phase crystals, which increase with increasing solvent evaporation temperature [20]. The vibrations bands at 1148 and 1295 cm^{-1} are assigned to symmetrical stretching mode of CF_2 and $CF_2(v_a)$ and $CF_2(r)$, respectively. Further, the vibration band at 838 cm^{-1} is characteristics of the β-phase. At a given polymer concentration (Fig. 5a), the vibration bands at 1148 and 1295 cm^{-1} increase with increasing solvent evaporation temperature and polymer/solvent ratio (Fig. 5b).

The specific bands at bands at 760 cm^{-1} and 838 cm^{-1} allow quantification of the α and β phase contents following the procedure presented in [20]. The phase content was calculated from the FTIR spectra by applying [20]:

$$F(\beta) = \frac{X_\beta}{X_\alpha + X_\beta} = \frac{A_\beta}{(K_\beta/K_\alpha)A_\alpha + A_\beta} \tag{4}$$

where, $F(\beta)$ represents the β-phase content; A_α and A_β the absorbencies at 760 and 838 cm^{-1}, corresponding to the α and β phase material; K_α and K_β are the absorption coefficient at the respective wave number and X_α and X_β the degree of crystallinity of each phase. The value of K_α is 6.1×10^4 and K_β is 7.7×10^4 cm^2/mol [20].

It is observed that the electroactive β-phase content decreases with increasing solvent evaporation temperature for a given initial polymer concentration, and also decreases with increasing polymer fraction in the initial

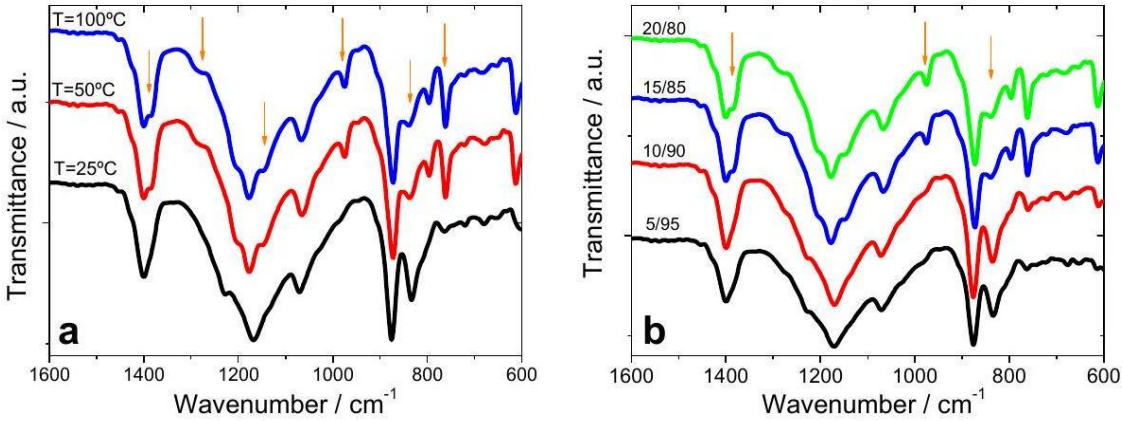

Fig. 5. FTIR-ATR spectra for a) samples prepared from 20wt% PVDF-HFP initial polymer concentration with solvent evaporated at different temperatures and b) samples prepared after solvent evaporation at T = 100°C for different initial polymer concentration in the PVDF-HFP/DMF system.

Table 2
β-phase content of the PVDF-HFP membranes as a function of the preparation conditions.

Samples	β-phase /% ± 2%
5/95, T = 100°C	75
10/90, T = 100°C	66
15/85, T = 100°C	22
20/80, T = 100°C	16
20/80, T = 50°C	24
20/80, T = 25°C	79

PVDF-HFP/DMF solution The evaporation rate is very important and affects the crystalline phase of PVDF and copolymers [20]. For low evaporation temperatures, crystallization is slow due to lower polymer chain mobility, which leads to nucleation of the electroactive β-phase [20] due to strong polar interactions. For higher evaporation temperatures, above 50°C, the evaporation rate is high, leading to crystallization of the material in the α-phase (Table 2). Regarding membranes evaporated at 100°C with different polymer concentrations, a decrease in the β-phase content with increasing polymer content in the initial solution (Table 2) is observed. This depends on the sample thickness (Fig. 1) and is explained by the solvent diffusion. Chinaglia et al., concluded the polymer concentration affects the diffusivity of the solvent in the dispersed phase at high

temperatures, and the evaporation rate grows faster than the solvent diffusivity through the polymeric solution [45].

Fig. 6 shows the DSC heating scans for the samples prepared from 20wt% PVDF-HFP initial concentration for different solvent evaporation temperatures as well as for the samples prepared after solvent evaporation at 100°C with different initial polymer concentrations. Independently of solvent evaporation temperature and initial polymer concentration, the melting behaviour is similar and characterized by a broad melting peak in the range 120 to 145°C.

The large melting peaks observed in Fig. 6 are due to the melting of the crystalline phase of the polymer. The differences observed in the shape of the peaks is attributed to the existence of more defective crystals and/or the different crystalline phase present in the PVDF-HFP polymer. The characteristic features of the materials obtained from the DSC scans of Fig. 6, melting temperature (T_m) and degree of crystallinity (χ) calculated after Equation 3, are summarized in Table 3. The melting temperature is similar, within experimental error, for all samples except for sample evaporated at room temperature (Fig. 6a), and also in line with the values reported in the literature for samples prepared with 12wt% of HFP [46]. Therefore, it is concluded that solvent evaporation temperature and initial polymer content in the solutions does not influence the melting temperature of the samples, hence leading to similar crystalline characteristics [45].

The degree of crystallinity, on the other hand, shows a stronger dependence on the processing conditions (Table

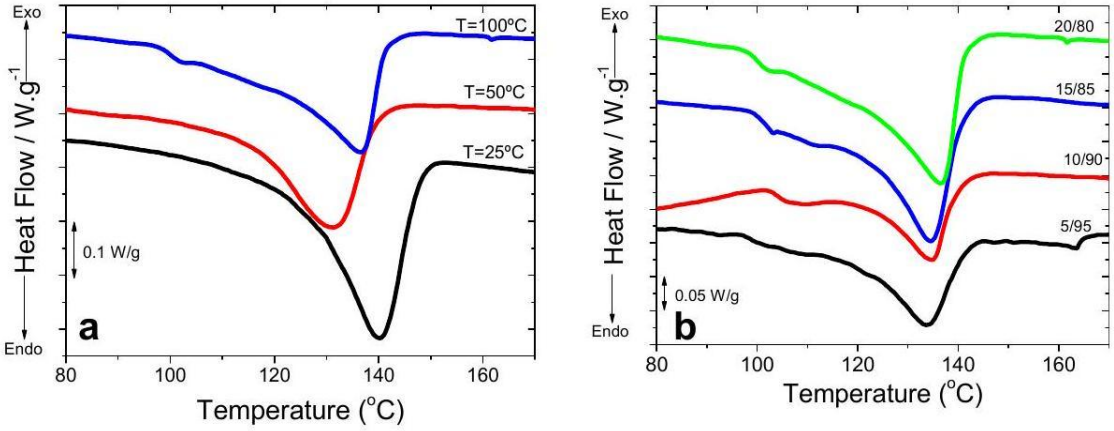

Fig. 6. DSC scans for the samples prepared with 20wt% initial polymer concentration evaporated at different temperatures a) and for the samples prepared after solvent evaporation at T = 100°C for different initial polymer concentration content in the PVDF-HFP/DMF system b).

Table 3
Melting temperature and degree of crystallinity of the membranes as a function of the preparation conditions.

Samples	T_f/ °C ± 1°C	χ/% ± 2%

5/95, T = 100°C	134	18
10/90, T = 100°C	135	14
15/85, T = 100°C	135	30
20/80, T = 100°C	138	35
20/80, T = 50°C	131	27
20/80, T = 25°C	140	33

3): whereas it is nearly independent of the solvent evaporation temperature, it shows a strong dependence on the initial polymer content, the degree of crystallinity increasing for increasing initial polymer concentration.

Decreasing initial polymer concentration leads to weaker polymer interaction during polymer crystallization due to the larger relative solvent content. This results in a lower degree of crystallinity [47].

Non-porous membranes are used in applications such as sensors and actuators and, therefore, it is important to characterize the dielectric and piezoelectric properties.

The dielectric behaviour (complex permittivity) of the samples is shown in Fig. 7. For PVDF homopolymer and its copolymers, it was reported that dielectric properties were anisotropic with respect to different crystal orientations [48]. The dielectric behaviour (ε', tan δ and σ') for the samples obtained after solvent evaporation at 50°C is the same as for the samples obtained after evaporation at 100 °C, so only the dielectric results for the PVDF-HFP membranes evaporated at 100°C are shown.

Fig. 7a) shows the variation of ε' for the samples with different polymer concentration evaporated at 100°C, as a function of frequency.

All PVDF-HFP membranes show similar behaviour of ε' as a function of frequency. The ε' decreases with increasing frequency due to slower dipole mobility. The differences observed in Fig. 7a) between membranes are correlated with the degree of crystallinity (Table 3), and thus with the initial polymer concentrations in the PVDF-HFP/DMF system.

The values of the dielectric constant, shown in the Fig. 7a) and 7d), are similar to the values of dielectric constant for PVDF homopolymer (α-phase, $\varepsilon' = 7$ and β -phase, $\varepsilon' = 12$) [49]. The value of ε' for PVDF-HFP polymer found in the literature ranges between 9.9 and 15, depending on the experimental conditions [46].

Regarding tan δ (Fig. 7b), it is observed that it increases with increasing frequency for all PVDF-HFP membranes, which can be attributed to the α_a relaxation process, i.e., micro-brownian movement of the amorphous phase chain segments or movement of crystalline-amorphous interphase chain segments [50].

The real part of the conductivity of the dielectric material can be calculated from the dielectric measurements presented in Fig. 7a) after Equation 5:

$$\sigma'(\omega) = \varepsilon_0 \omega \varepsilon''(\omega) \quad (5)$$

where ε_0 is the permittivity of free space, $\omega = 2\pi f$ is the angular frequency and $\varepsilon''(\omega) = \varepsilon' \tan\ \delta$ is the frequency dependent imaginary part of the dielectric permittivity [51].

The $\sigma'(\omega)$ values for the PVDF-HFP membranes at different polymer concentrations as a function of frequency are presented in Fig. 7c). For all PVDF-HFP membranes, the conductivity increases with increasing of frequency in a similar way.

Fig. 6a shows that the dielectric constant depends on the evaporation temperature, i.e., increases with the increasing temperature and depends on the crystalline phase present in the polymer (α - and β-phase). At the same polymer concentration, 20wt%, dielectric constant increases with increasing of α-phase ($T = 50\ ^\circ C, \alpha$ phase $= 76\%$ and $T = 100^\circ C, \alpha$-phase $= 84\%$).

Poling of the material is a critical step in the optimization of the piezoelectric response of the samples in the electroactive phase [20,52,53], the final material response strongly depending on processing conditions and resulting crystal microstructure structure. In this way, the piezoelectric response, as evaluated by the d_{33} piezoelectric coefficient, was optimized as a function of poling temperature and concentration as shown in Fig. 8.

Generally, the piezoelectric coefficient increases with increasing poling temperature, as temperature increases the mobility of the molecular chains, allowing a more effective orientation of the molecular dipoles though the interaction with the applied electric field [54]. The maximum poling temperature used in the work is below

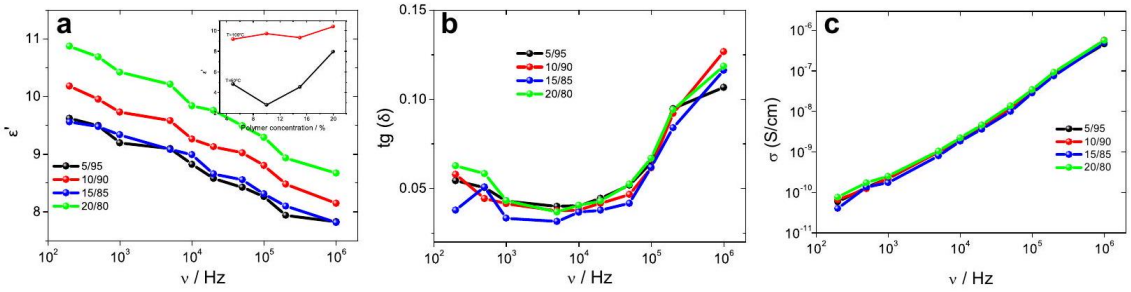

Fig. 7. Electrical response for the samples obtained after solvent evaporation at $T = 100^\circ C$ with different polymer concentrations in the PVDF-HFP/DMF system: a) dielectric constant, b) tan δ and c) conductivity. Insert of a) Variation of the dielectric constant as a function of polymer concentration for at 1 kHz .

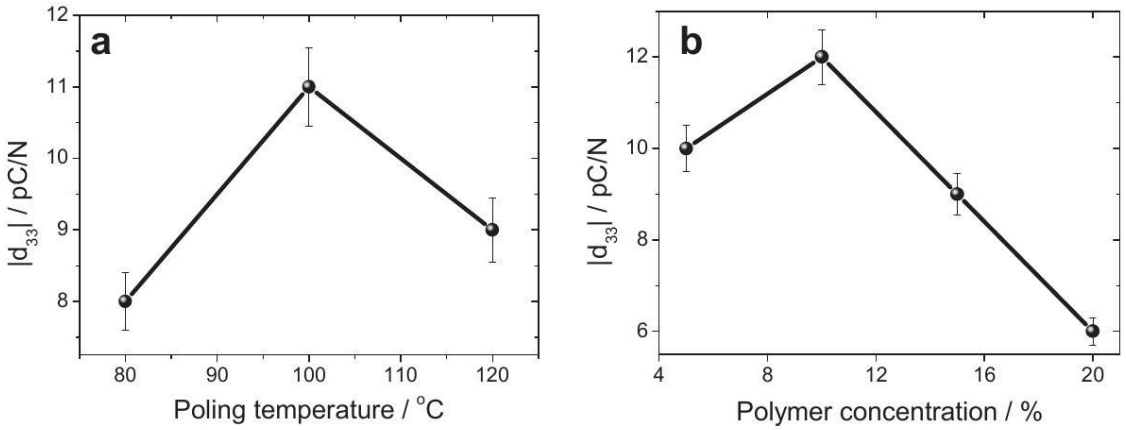

Fig. 8. a) Modulus of the piezoelectric d_{33} coefficient for the membrane with 20wt% of PVDF-HFP initial concentration and solvent evaporation temperature of 50°C as a function of poling temperature and b) modulus of the d_{33} piezoelectric coefficient for the solvent evaporation temperature of 100 °C and poling temperature of 100°C as a function of polymer concentrations in the PVDF-HFP/DMF system.
the melting temperature, $T_m \sim 131 - 140$ °C, in order to prevent sample degradation. Fig. 8a) shows the $|d_{33}|$ behaviour as a function of poling temperature for the membrane with 20wt% PVDF-HFP initial concentration and solvent evaporation temperature of 50 °C. The observed behaviour is representative of the remaining samples studied in this work.

The piezoelectric coefficient is negative, and its modulus $|d_{33}|$ increases with increasing poling temperature from ~ 8 up to $\sim 11\text{pC/N} \pm 2\text{pC/N}$ by poling at 80 and 100 °C respectively. For increasing poling temperature up to 120°C, the $|d_{33}|$ decreases to $\sim$ 9pC/N.

In this way, as temperature increases for a given poling field, the molecular chain mobility increases, inducing better alignment of the dipolar moments with the applied electric field and, therefore, an increase of the piezoelectric response [55]. This behaviour is hindered close to the melting temperature due to irreversible effects on the crystalline microstructure [56].

Fig. 8b) shows the behaviour of the $|d_{33}|$ coefficient as a function of polymer concentration in the PVDF-HFP/DMF system for solvent evaporation temperature of 100°C.

The modulus of the piezoelectric d_{33} coefficient decreases with increasing polymer concentration in the PVDF-HFP/DMF system. This behavior is mainly attributed to the different electroactive β-phase content within the PVDF-HFP polymer samples that affects the piezoelectric properties of the polymer: the larger the β-phase content the larger the piezoelectric response of the material [52]. The β-phase of the samples is responsible for the piezoelectric properties. According to Fig. 8b), the $|\ d_{33}\ |$ behaviour follows the same trend as the β-phase content in the PVDFHFP, which depends on the polymer concentration in the PVDF-HFP/DMF system.

The values of the d_{33} determined in this work are in accordance with the values observed in the literature, i.e, He et al., $|d_{33}|/\text{pC/N} = 5.4 - 12.6$ [57] for maximum field of 250MV/m at room temperature and Huan et al. $|d_{33}|/\text{pC/ N} = 20 - 24$[58] at poling fields from 20 to 160MV/m.

Discussion

The morphology, β-phase content and thermal properties of PVDF-HFP samples depend on the initial polymer concentration and solvent evaporation temperature, as shown in Figs. 2, 5 and 6. The microstructural variations of the PVDF-HFP membranes shown in Fig. 2 are due to the phase separation during the crystallization process, as demonstrated in the phase diagram of Fig. 9. By solvent evaporation at room temperature, the membranes exhibit a degree of porosity that depends on the polymer concentration, as illustrated in Fig. 3. Regardless of the experimental conditions (PVDF-HFP concentration, 5-20 wt% and evaporation solvent temperature, $\mathrm{T} = 25°\mathrm{C}, \mathrm{T} = 50°\mathrm{C}$ and $\mathrm{T} = 100°\mathrm{C}$), the membranes show β-phase contents above 79% (Fig. 5 and Table 2). The degree of crystallinity determined by DSC scans (Fig. 6) ranges between 11 and 35%, depending on the polymer concentration and solvent evaporation temperature, which may be due to the deferral of the liquid-liquid demixing process. The dielectric and piezoelectric properties are correlated with the degree of crystallinity and β-phase content. The variation of these properties is understood in terms of the initial position of the solution the PVDF-HFP/DMF phase diagram (Fig. 9).

The isothermal evaporation process can be described by the Flory-Huggins theory [59].

The Gibbs free energy fluctuations for binary systems (polymer/solvent) are described by [60]:

$$\frac{\Delta G}{RT} = \frac{\phi'}{n} \ln\ \phi' + (1 - \phi') \ln\,(1 - \phi') + \chi_{12}\phi'(1 - \phi') \tag{6}$$

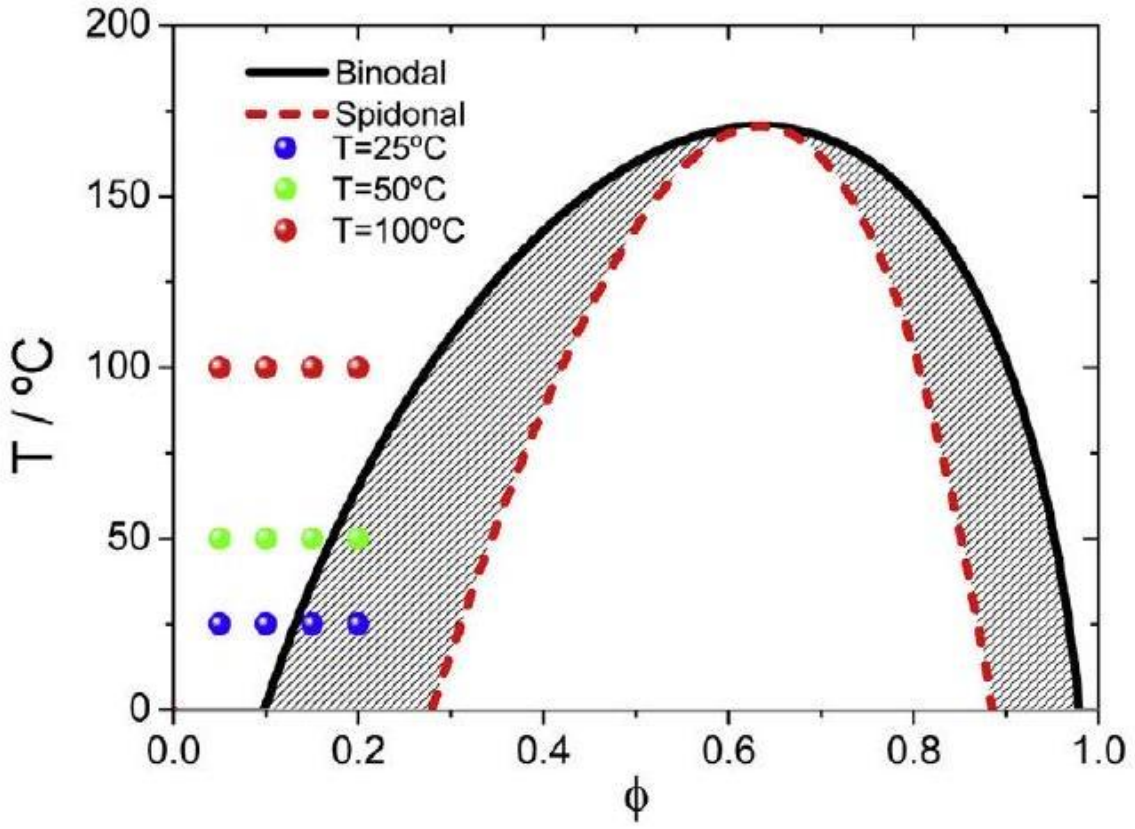

Fig. 9. Phase diagram for the PVDF-HFP/DMF system. where n is the degree of polymerization, ϕ' is the polymer volume fraction and χ_{12} is the Flory-Huggins parameter for a binary mixture.

The Flory-Huggins parameter χ_{12} in order to temperature is determined by.

$$\chi_{12} = \frac{v_0}{RT}\delta^2 \tag{7}$$

where R is the gas constant, v_0 is the molar volume of the solvent, T is the temperature, and δ is the solubility parameter.

Through the Flory-Huggins theory (Equation 6), the phase diagram for the PVDF-HFP/DMF system was constructed using $v_0 = 77.4\ \mathrm{cm}^3.\mathrm{mol}^{-1}$ (DMF volume molar), N = 3.5 (Solvay datasheet) and the solubility parameters $\left(\delta_{PVDF-HFP} = 17.2\mathrm{MPa}^{1/2}, \delta_{DMF} = 24.7\mathrm{MPa}^{1/2}\right)$[61,62].

The phase diagram is represented in Fig. 9 and shows the regions of stability, metastability and instability of the polymer solution. These regions are separated by the binodal and the spinodal lines, and the phase separation of the PVDF-HFP/DMF system can be controlled through the initial polymer concentration and the solvent evaporation temperature.

The metastable region between the spinodal and binodal lines is referred to as the nucleation and growth region. The phase separation occurs either by spinodal decomposition or by nucleation and growth region (metastable region). The initial

position of the PVDF-HFP/DMF solution in the phase diagram (Fig. 9) for the preparation of the membranes is represented by the circle.

At room temperature, for the different polymer/solvent ratios, the microstructure formation is governed by competition between the phase separation dynamics and the evaporation of the solvent. However, when polymer concentration is increased, the system transits from the unstable (5wt% of PVDF-HFP) to metastable region (20wt% of PVDF-HFP) in which the process is dominated by nucleation and growth, leading to PVDF-HFP membranes with different degree of porosity (see of Figs. 2-3).

For a given polymer/solvent ratio (20/80) at different solvent temperatures (20°C and 100°C), the system passes from the metastable region to the one-phase region (homogeneous microstructure) and no porous microstructure is observed (Fig. 2). This is also observed for others polymer/solvent ratios. At a given evaporation temperature (T = 100°C), the piezoelectric coefficient depends on the polymer concentration and is related to β-phase content and degree of crystallinity [52]. The |d33| coefficient decreases with decreasing of the β-phase content and shows lower variation with the degree of crystallinity of the samples.

Conclusions

Poly(vinylidene fluoride-co-hexafluropropylene) P(VDFHFP), membranes were prepared by TIPS from DMF solutions varying initial polymer concentration and solvent evaporation temperature.

PVDF-HFP membranes with a wide range of different morphologies and degrees of porosity were produced.

The experimental results are correlated with the initial position of the solution in the phase diagram for the binary system described by the Flory-Huggins theory. After solvent evaporation at room temperature, the samples show a porous microstructure with varying degree of porosity, attributed to the spinodal decomposition of the liquid-liquid phase separation. These PVDF-HFP membranes present different β-phase content and degree of crystallinity that can be controlled through the polymer concentration and evaporation solvent temperature. These variations depend on the positions of the membranes in the phase diagram determined by PVDF-HFP/ DMF system.

Both degree of crystallinity and β-phase content also determine the piezoelectric response of the PVDF-HFP membranes, leading to suitable samples for applications in battery separator membranes, sensors and actuators.

Acknowledgments

This work is funded by FEDER funds through the "Programa Operacional Factores de Competitividade COMPETE" and by national funds from FCT - Fundação para a Ciência e a Tecnologia, in the framework of the strategic project Strategic Project PEST-C/FIS/UI607/2011 and PEst-C/ QUI/UI0686/2013). The authors also thank funding from Matepro -Optimizing Materials and Processes", ref. NORTE-07-0124-FEDER-000037", co-funded by the "Programa Operacional Regional do Norte" (ON. 2 - O Novo Norte), under the "Quadro de Referência Estratégico Nacional" (QREN), through the

"Fundo Europeu de Desenvolvimento Regional" (FEDER), and grants SFRH/BD/66930/2009 (J.N.P.) and SFRH/BD/68499/2010 (C.M.C.). The authors thank Solvay for kindly supplying the high quality materials.

References

[1] F. Liu, N.A. Hashim, Y. Liu, M.R.M. Abed, K. Li, Progress in the production and modification of PVDF membranes, Journal of Membrane Science 375 (2011) 1-27.
[2] P. Van De Witte, P.J. Dijkstra, J.W.A. Van Den Berg, J. Feijen, Phase separation processes in polymer solutions in relation to membrane formation, Journal of Membrane Science 117 (1996) 1-31.
[3] A.P. Echavarría, C. Torras, J. Pagán, A. Ibarz, Fruit Juice processing and membrane technology application, Food Engineering Reviews 3 (2011) 136-158.
[4] H.S. Thiam, W.R.W. Daud, S.K. Kamarudin, A.B. Mohammad, A.A.H. Kadhum, K.S. Loh, E.H. Majlan, Overview on nanostructured membrane in fuel cell applications, International Journal of Hydrogen Energy 36 (2011) 3187-3205.
[5] R. Miao, B. Liu, Z. Zhu, Y. Liu, J. Li, X. Wang, Q. Li, PVDF-HFP-based porous polymer electrolyte membranes for lithium-ion batteries, Journal of Power Sources 184 (2008) 420-426.
[6] C. Feng, K.C. Khulbe, T. Matsuura, S. Tabe, A.F. Ismail, Preparation and characterization of electro-spun nanofiber membranes and their possible applications in water treatment, Separation and Purification Technology 102 (2013) 118-135.
[7] G.R. Guillen, Y. Pan, M. Li, E.M.V. Hoek, Preparation and characterization of membranes formed by nonsolvent induced phase separation: a review, Industrial & Engineering Chemistry Research 50 (2011) 3798-3817.
[8] M. Mulder, Basic Principles of Membrane Technology, Springer, 1996.
[9] D. Li, W.B. Krantz, A.R. Greenberg, R.L. Sani, Membrane formation via thermally induced phase separation (TIPS): model development and validation, Journal of Membrane Science 279 (2006) 50-60.
[10] N. Ghasem, M. Al-Marzouqi, N. Abdul Rahim, Modeling of CO2 absorption in a membrane contactor considering solvent evaporation, Separation and Purification Technology 110 (2013) 1-10.
[11] A. Venault, Y. Chang, D.-M. Wang, D. Bouyer, A. Higuchi, J.-Y. Lai, PEGylation of anti-biofouling polysulfone membranes via liquidand vapor-induced phase separation processing, Journal of Membrane Science 403-404 (2012) 47-57.
[12] S.K. Yong, J.K. Hyo, Y.K. Un, Asymmetric membrane formation via immersion precipitation method. I. Kinetic effect, Journal of Membrane Science 60 (1987) 219-232.
[13] L. Zeman, T. Fraser, Formation of air-cast cellulose acetate membranes. Part I. Study of macrovoid formation, Journal of Membrane Science 84 (1993) 93-106.
[14] M. Liu, Y.M. Wei, Z.L. Xu, R.Q. Guo, L.B. Zhao, Preparation and characterization of polyethersulfone microporous membrane via thermally induced phase separation with low critical solution temperature system, Journal of Membrane Science 437 (2013) 169-178.
[15] Y.H. Tang, Y.D. He, X.L. Wang, Three-dimensional analysis of membrane formation via thermally induced phase separation by dissipative particle dynamics simulation, Journal of Membrane Science 437 (2013) 40-48.
[16] Y. Zhao, Q. Lu, D. Chen, Y. Wei, Superhydrophobic modification of polyimide films based on gold-coated porous silver nanostructures and self-assembled monolayers, Journal of Materials Chemistry 16 (2006) 4504-4509.
[17] Y. Zhou, Z. Wang, Q. Zhang, X. Xi, J. Zhang, W. Yang, Equilibrium and

thermodynamic studies on adsorption of BSA using PVDF microfiltration membrane, Desalination 307 (2012) 61-67.
[18] A. Gugliuzza, E. Drioli, PVDF and HYFLON AD membranes: ideal interfaces for contactor applications, Journal of Membrane Science 300 (2007) 51-62.
[19] E. Drioli, A. Ali, S. Simone, F. Macedonio, S.A. Al-Jlil, F.S. Al Shabonah, H.S. Al-Romaih, O. Al-Harbi, A. Figoli, A. Criscuoli, Novel PVDF hollow fiber membranes for vacuum and direct contact membrane distillation applications, Separation and Purification Technology 115 (2013) 27-38.
[20] P. Martins, A.C. Lopes, S. Lanceros-Mendez, Electroactive phases of poly(vinylidene fluoride): determination, processing and applications, Progress in Polymer Science 39 (2014) 683-706.
[21] Y. Ding, P. Zhang, Z. Long, Y. Jiang, F. Xu, W. Di, The ionic conductivity and mechanical property of electrospun P(VdF – HFP)/PMMA membranes for lithium ion batteries, Journal of Membrane Science 329 (2009) 56-59.
[22] J.-H. Cao, B.-K. Zhu, Y.-Y. Xu, Structure and ionic conductivity of porous polymer electrolytes based on PVDF-HFP copolymer membranes, Journal of Membrane Science 281 (2006) 446-453.
[23] W. Pu, X. He, L. Wang, C. Jiang, C. Wan, Preparation of PVDF-HFP microporous membrane for Li-ion batteries by phase inversion, Journal of Membrane Science 272 (2006) 11-14.
[24] M.C. García-Payo, M. Essalhi, M. Khayet, Effects of PVDF-HFP concentration on membrane distillation performance and structural morphology of hollow fiber membranes, Journal of Membrane Science 347 (2010) 209-219.
[25] M. Akkoyun, C. Carrot, B. Blottière, Ternary diagrams of poly(vinylidene fluoride) and poly[(vinylidene fluoride)-cohexafluoropropene] in propylene carbonate and dimethyl sulfoxide, Macromolecular Chemistry and Physics 213 (2012) 587-593.
[26] K. Smolders, A.C.M. Franken, Terminology for membrane distillation, Desalination 72 (1989) 249-262.
[27] S. Lanceros-Méndez, J.F. Mano, A.M. Costa, V.H. Schmidt, FTIR and DSC studies of mechanically deformed β-PVDF films, Journal of Macromolecular Science, Part B 40 (2001) 517-527.
[28] D.C. Bassett, Developments in Crystalline Polymers, Applied Science Publishers, 1982.
[29] T.R. Dargaville, M. Celina, P.M. Chaplya, Evaluation of piezoelectric poly(vinylidene fluoride) polymers for use in space environments. I. Temperature limitations, Journal of Polymer Science Part B: Polymer Physics 43 (2005) 1310-1320.
[30] D.-J. Lin, C.-L. Chang, F.-M. Huang, L.-P. Cheng, Effect of salt additive on the formation of microporous poly(vinylidene fluoride) membranes by phase inversion from LiClO4/Water/DMF/PVDF system, Polymer 44 (2003) 413-422.
[31] V. Sencadas, C.M. Costa, J.L. Gómez Ribelles, S. Lanceros-Mendez, Isothermal crystallization kinetics of poly(vinylidene fluoride) in the α-phase in the scope of the Avrami equation, Journal of Materials Science 45 (2010) 1328-1335.
[32] M.J. Koh, H.Y. Hwang, D.J. Kim, H.J. Kim, Y.T. Hong, S.Y. Nam, Preparation and characterization of porous PVdF-HFP/clay nanocomposite membranes, Journal of Materials Science & Technology 26 (2010) 633-638.
[33] X. Wang, L. Zhang, D. Sun, Q. An, H. Chen, Formation mechanism and crystallization of poly(vinylidene fluoride) membrane via immersion precipitation method, Desalination 236 (2009) 170-178.
[34] R. Magalhães, N. Durães, M. Silva, J. Silva, V. Sencadas, G. Botelho, J.L. Gómez Ribelles, S. Lanceros-Méndez, The role of solvent evaporation in the microstructure of

electroactive β-poly(vinylidene fluoride) membranes obtained by isothermal crystallization, Soft Materials 9 (2010) 1-14.
[35] P. Dietz, P.K. Hansma, O. Inacker, H.-D. Lehmann, K.-H. Herrmann, Surface pore structures of micro- and ultrafiltration membranes imaged with the atomic force microscope, Journal of Membrane Science 65 (1992) 101-111.
[36] L.-P. Zhu, J.-Z. Yu, Y.-Y. Xu, Z.-Y. Xi, B.-K. Zhu, Surface modification of PVDF porous membranes via poly(DOPA) coating and heparin immobilization, Colloids and Surfaces B: Biointerfaces 69 (2009) 152-155.
[37] P.M. Martins, S. Ribeiro, C. Ribeiro, V. Sencadas, A.C. Gomes, F.M. Gama, S. Lanceros-Mendez, Effect of poling state and morphology of piezoelectric poly(vinylidene fluoride) membranes for skeletal muscle tissue engineering, RSC Advances 3 (2013) 17938-17944.
[38] D. Kumar, M. Suleman, S.A. Hashmi, Studies on poly(vinylidene fluoride-co-hexafluoropropylene) based gel electrolyte nanocomposite for sodium-sulfur batteries, Solid State Ionics 202 (2011) 45-53.
[39] V. Aravindan, P. Vickraman, Nanoparticulate Al0(0H)[sub n] filled polyvinylidenefluoride-co-hexafluoropropylene based microporous membranes for lithium ion batteries, Journal of Renewable and Sustainable Energy 1 (2009) 023108.
[40] S. Ramesh, S.-C. Lu, I. Vankelecom, BMIMTf ionic liquid-assisted ionic dissociation of MgTf in P(VdF-HFP)-based solid polymer electrolytes, Journal of Physics and Chemistry of Solids 74 (2013) 1380-1386.
[41] C.-H. Du, B.-K. Zhu, Y.-Y. Xu, The effects of quenching on the phase structure of vinylidene fluoride segments in PVDF-HFP copolymer and PVDF-HFP/PMMA blends, J Mater Sci 41 (2006) 417-421.
[42] V. Aravindan, P. Vickraman, T.P. Kumar, Polyvinylidene fluo-ride-hexafluoropropylene (PVdF-HFP)-based composite polymer electrolyte containing LiPF3(CF3CF2)3, Journal of Non-Crystalline Solids 354 (2008) 3451-3457.
[43] N. Ataollahi, A. Ahmad, H. Hamzah, M.Y.A. Rahman, N.S. Mohamed, Preparation and characterization of PVDF-HFP/MG49 based polymer blend electrolyte, International Journal of the Electrochemical Society 7 (2012) 6693-6703.
[44] M. Ulaganathan, R. Nithya, S. Rajendran, S. Raghu, Li-ion conduction on nanofiller incorporated PVdF-co-HFP based composite polymer blend electrolytes for flexible battery applications, Solid State Ionics 218 (2012) 7-12.
[45] D.L. Chinaglia, R. Gregorio, J.C. Stefanello, R.A. Pisani Altafim, W. Wirges, F. Wang, R. Gerhard, Influence of the solvent evaporation rate on the crystalline phases of solution-cast poly(vinylidene fluoride) films, Journal of Applied Polymer Science 116 (2010) 785-791.
[46] A.C. Jayasuriya, A. Schirokauer, J.I. Scheinbeim, Crystal-structure dependence of electroactive properties in differently prepared poly(vinylidene fluoride/hexafluoropropylene) copolymer films, Journal of Polymer Science Part B: Polymer Physics 39 (2001) 2793-2799.
[47] M.G. Buonomenna, P. Macchi, M. Davoli, E. Drioli, Poly(vinylidene fluoride) membranes by phase inversion: the role the casting and coagulation conditions play in their morphology, crystalline structure and properties, European Polymer Journal 43 (2007) 1557-1572.
[48] M.A. Marcus, Orientation effects on dielectric and piezoelectric properties of polyvinylidene fluoride films, Electrical Insulation, IEEE Transactions On EI-21 (1986) 519-523.
[49] V. Sencadas, S. Lanceros-Méndez, R. Sabater i Serra, A. Andrio Balado, J.L. Gómez Ribelles, Relaxation dynamics of poly(vinylidene fluoride) studied by dynamical mechanical measurements and dielectric spectroscopy, The European Physical Journal E

35 (2012) 1-11.
[50] H. Arisawa, O. Yano, Y. Wada, Dielectric loss of poly(vinylidene fluoride) at low temperatures and effect of poling on the low temperature loss, Ferroelectrics 32 (1981) 39-41.
[51] F. Kremer, A. Schönhals, Broadband Dielectric Spectroscopy, Springer, 2003.
[52] J. Gomes, J.S. Nunes, V. Sencadas, S. Lanceros-Mendez, Influence of the β-phase content and degree of crystallinity on the piezo- and ferroelectric properties of poly(vinylidene fluoride), Smart Materials and Structures 19 (2010) 065010.
[53] V.F. Cardoso, G. Minas, C.M. Costa, C.J. Tavares, S. Lanceros-Mendez, Micro and nanofilms of poly(vinylidene fluoride) with controlled thickness, morphology and electroactive crystalline phase for sensor and actuator applications, Smart Materials and Structures 20 (2011) 087002.
[54] M. Inoue, Y. Tada, K. Suganuma, H. Ishiguro, Variations in polymeric structure of ferroelectric poly(vinylidene fluoride) films during annealing at various temperatures, Journal of Applied Polymer Science 111 (2009) 2837-2843.
[55] V.F. Cardoso, C.M. Costa, G. Minas, S. Lanceros-Mendez, Improving the optical and electroactive response of poly(vinylidene fluo-ride-trifluoroethylene) spin-coated films for sensor and actuator applications, Smart Materials and Structures 21 (2012) 085020.
[56] D. Damjanovic, M. Demartin, Contribution of the irreversible displacement of domain walls to the piezoelectric effect in barium titanate and lead zirconate titanate ceramics, Journal of Physics: Condensed Matter 9 (1997) 4943.
[57] X. He, K. Yao, B.K. Gan, Phase transition and properties of a ferroelectric poly(vinylidene fluoride-hexafluoropropylene) copolymer, Journal of Applied Physics 97 (2005).
[58] Y. Huan, Y. Liu, Y. Yang, Simultaneous stretching and static electric field poling of poly(vinylidene fluoride-hexafluoropropylene) copolymer films, Polymer Engineering & Science 47 (2007) 1630-1633.
[59] J.S. Higgins, J.E.G. Lipson, R.P. White, A simple approach to polymer mixture miscibility, Philosophical Transactions of the Royal Society A: Mathematical, Physical and Engineering Sciences 368 (2010) 1009-1025.
[60] M. Rubinstein, R.H. Colby, Polymer Physics, OUP Oxford, 2003.
[61] A.F.M. Barton, CRC Handbook of Solubility Parameters and Other Cohesion Parameters, Second ed., Taylor & Francis, 1991.
[62] X. Tian, X. Jiang, Poly(vinylidene fluoride-co-hexafluoropropene) (PVDF-HFP) membranes for ethyl acetate removal from water, Journal of Hazardous Materials 153 (2008) 128-135.